Temperature dependence of the magnetic Compton profile of ferrimagnetic $DyFe_2$ and $ErFe_2$

1995 J. Phys.: Condens. Matter 7 389

(http://iopscience.iop.org/0953-8984/7/2/017)

J. Phys.: Condens. Matter 7 (1995) 389–400. Printed in the UK

Temperature dependence of the magnetic Compton profile of ferrimagnetic $DyFe_2$ and $ErFe_2$

P K Lawson†, J E McCarthy†, M J Cooper†, E Żukowski‡, D N Timms§, F Itoh‖, H Sakurai‖, Y Tanaka¶, H Kawata†† and M Ito‡‡

† Department of Physics, University of Warwick, Coventry CV4 7AL, UK
‡ Institute of Physics, Warsaw University Branch, ulica Lipowa 41, 15-424 Białystok, Poland
§ Department of Applied Physics, University of Portsmouth, Portsmouth PO1 2DZ, UK
‖ Department of Electrical and Electronic Engineering, Gunma University, Kiryu 376, Japan
¶ The Institute for Physical and Chemical Research (RIKEN), Wako-shi, Saitama 351-01, Japan
†† Photon Factory, KEK, Oho, Tsukuba, Ibaraki 305, Japan
‡‡ Faculty of Science, Himeji Institute of Technology, Kanaji 1479-1, Kanagori, Hyogo 678-12, Japan

Received 10 October 1994

Abstract. The spin moments in $DyFe_2$ and $ErFe_2$ samples have been determined from magnetic Compton scattering experiments performed at the KEK Accumulation Ring with 47.1 keV circularly polarized synchrotron radiation at temperatures 50–355 K. The polycrystalline samples were mounted in a cryostat and magnetized by an electromagnet producing a magnetic field of 0.5 T. The magnetic field was aligned parallel to the x-ray scattering vector and the scattering angle was fixed at 160°. The good signal averaging associated with the use of an electromagnet facilitated the analysis of the magnetic Compton profiles of $DyFe_2$ and $ErFe_2$ in terms of a combination of rare-earth 4f, diffuse and iron 3d free-atom Compton profiles. The temperature dependence of the total spin moment mirrors the corresponding dependence of the rare-earth 4f moment. The rare-earth orbital moments have been deduced by combining the Compton data with bulk magnetization measurements.

1. Introduction

There is obvious interest in any experimental technique that can differentiate between spin and orbital contributions to magnetization or separate the moments on individual sites. This is especially true in materials where the net moment is derived from the difference between two contributions because knowledge of the total provides little empirical information about the individual values. Non-resonant x-ray diffraction with polarized synchrotron radiation may provide this detail at some future date but its potential is yet to be realized. In this paper we explore the extent to which a technique that isolates the spin contribution, namely magnetic Compton scattering, when coupled with bulk magnetization data, can provide information on site-specific spin and orbital moments. Charge and spin-dependent momentum distributions can be probed in Compton scattering experiments; the latter requiring circularly polarized photons [1–6]. The quantities measured are the charge Compton profile, $J(p_z)$, and the magnetic Compton profile, $J_{mag}(p_z)$. Compton experiments are undertaken within the so-called impulse approximation (IA) where the energy transfer upon scattering must be large compared to the binding energy of the target electrons [7]. Within the IA, the scattering cross-section is related directly to the charge Compton profile,

0953-8984/95/020389+12$19.50

$J(p_z)$, which is defined as the projection of the electron momentum density distribution, $n(p)$, along the scattering vector, usually taken as the z-axis of a Cartesian coordinate system:

$$J(p_z) = \int\int n(p)\, \mathrm{d}p_x \mathrm{d}p_y. \tag{1}$$

In equation (1) $n(p)$ is the sum, $n^{\uparrow}(p)+n^{\downarrow}(p)$, of the electron momentum density distribution in the sub-bands. This associated cross-section is independent of the polarization of the probe and is a slowly varying function of energy. Measurements of $J(p_z)$ are normally performed with unpolarized gamma rays at energies of 60 keV [8] or above, depending on the isotopic source, or with synchrotron radiation at the highest energy for which there is adequate flux [9]. The charge Compton profile is subject to the normalization condition

$$\int_{-\infty}^{+\infty} J(p_z)\, \mathrm{d}p_z = N \tag{2}$$

where N is the number of electrons per formula unit in the target. Magnetic Compton scattering arises when circular polarization is used to yield a real interference term between the charge and magnetic scattering amplitudes. The magnetic Compton profile, $J_{\mathrm{mag}}(p_z)$, is defined as a projection of the momentum distribution along the scattering vector of the unpaired spin electrons

$$J_{\mathrm{mag}}(p_z) = \int\int \left(n^{\uparrow}(p) - n^{\downarrow}(p)\right) \mathrm{d}p_x\, \mathrm{d}p_y. \tag{3}$$

It is subject to the normalization condition

$$\int_{-\infty}^{+\infty} J_{\mathrm{mag}}(p_z)\, \mathrm{d}p_z = F_S \tag{4}$$

where F_S is numerically equal to the spin moment per formula unit in Bohr magnetons. The amplitude of the magnetic scattering is proportional to the momentum transfer and can be maximized by using the highest energy and highest scattering angle practicable. The cross-section associated with this process, for the scattering geometry shown in figure 1, can be given by the following equations:

$$\frac{\mathrm{d}^2\sigma}{\mathrm{d}\Omega\, \mathrm{d}E_2} = r_0^2 \left(\frac{E_2}{E_1}\right) \left[f_1 J(p_z) + f_2 g P_c S(\alpha) J_{\mathrm{mag}}(p_z)\right] \tag{5}$$

$$f_1 = 1 + \cos^2\theta + \frac{E_1 - E_2}{mc^2}(1 - \cos\theta) + P_l \sin^2\theta \qquad f_2 = -(1 - \cos\theta) \tag{6}$$

$$S(\alpha) = \sigma \left(\cos\alpha \cos\theta + \frac{E_2}{E_1}\cos(\theta - \alpha)\right) \tag{7}$$

where r_0 is the classical electron radius and P_l is the degree of linear polarization. The definition of linear polarization is such that $P_l = -1$ for a beam completely linearly polarized parallel to the plane of scattering; P_c is the degree of circular polarization and the quantity

$s = \pm 1$ depends on the direction of the magnetic field. Other quantities are defined in figure 1. The magnetic effect is defined by the ratio $R\ (I^+ - I^-)/(I^+ + I^-)$ where I^+ and I^- represent the integrated Compton intensities for opposing sample magnetizations. At typical photon energies of 50 keV the magnetic effect amounts to 1% of the charge scattering for Fe, for example, but is less than 0.15% for $DyFe_2$ and $ErFe_2$. The spin-dependent profile, $J_{mag}(p_z)$, is isolated by reversing the direction of magnetization and subtracting the spin-up and spin-down signals. It has recently been shown [10, 11] that no orbital scattering contribution is detected in magnetic Compton experiments carried out within the IA. In a previous experiment the spin moments in $HoFe_2$ were investigated using a superconducting magnet to flip the spins. This led to poor signal averaging because long switching times were needed to ramp the magnet current. To overcome this problem in the present study a specially designed electromagnet, capable of fast switching, was chosen; this resulted in a marked improvement in the signal averaging. Since electromagnets do not produce the high fields that are obtainable from superconducting magnets, the samples analysed must have relatively soft magnetic moments and the sintered powder samples of $DyFe_2$ and $ErFe_2$ used in these experiments fall into this category. They are readily available compounds falling either side in the periodic table of the previously investigated sample, $HoFe_2$.

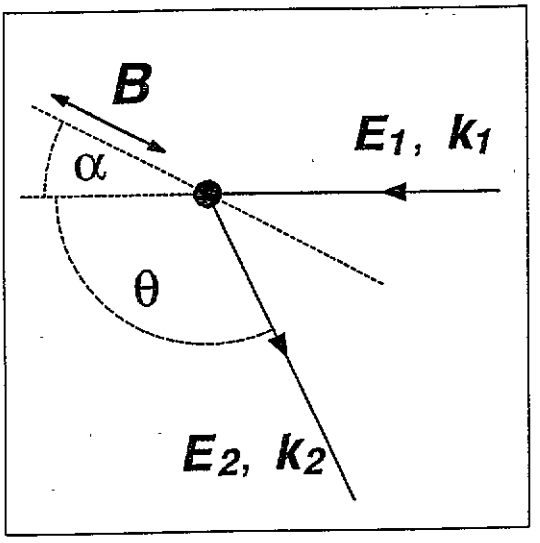

Figure 1. The scattering geometry of the experiment: k_1 and k_2 are the wave vectors of the incident and scattered photons which have energies E_1 and E_2 respectively. The arrows indicate the alternate directions of the external magnetic field, B (parallel and antiparallel to the scattering vector); θ is the scattering angle (160°) and α the angle between the incident beam and the direction of the applied magnetic field (9°).

2. Experiments

The experiments were performed at the ARNE-1 station on the Accumulation Ring at KEK in Japan using elliptically polarized synchrotron radiation from an elliptical multipole wiggler [12]. The white beam was monochromated and focused by a water cooled, doubly

bent silicon [111] monochromator. The incident beam energy was chosen to be 47.1 keV, an energy which is below the K-shell absorption edges of both Er and Dy and one which limits the K-shell fluorescence to that arising from photons passed by the higher harmonics of the monochromator. Fluxes at the sample position were of the order of 1010 photons s^{-1} mm^{-2} and the degree of circular polarization was around 0.6 [12–14]. The beam size at the sample position was approximately 9×2 mm. Both sintered powder samples measured $24 \times 9 \times 1$ mm and were mounted in a cryostat which in turn sat between the pole pieces of an electromagnet that was capable of producing a magnetic field of approximately 0.5 T. The field was aligned parallel to the x-ray scattering vector and the scattering angle was fixed at 160°. The data were collected using a thirteen-element germanium solid-state detector, each element having its own power supply and counting chain which is adjusted to ensure identical energy calibrations. Unfortunately six of the thirteen detector elements had either poor energy resolution or were not functioning at all leaving only seven detectors for use in this investigation. The counting rate per detector was of the order of 35 000 cps with initial ring currents and lifetimes of 30 mA and 4 h respectively. Fast analogue-to-digital converters were used ensuring no pile-up problems. As usual, the elastic line intensities were used to normalize the data for beam instability to ensure that spin-up and spin-down data were collected with the same number of incoming photons. The magnetic field in the sample was reversed in the sequence [+, −, −, +] where (+) and (−) represent the relative directions of the magnetic field (+ being parallel to the scattering vector and vice versa). A switching time of the order of two seconds and a dwell time of fifteen seconds was used to ensure good signal averaging. This is in contrast to our earlier measurement on $HoFe_2$ where the use of a superconducting magnet dictated switching times of two minutes and a dwell time of just under three minutes resulting in poor signal averaging. Measurements were performed on each sample at several temperatures in the range 50 K to 355 K and each corresponded to approximately five hours of synchrotron beamtime. This in turn equates to at least ten hours of real time due to the operational nature of the Accumulation Ring.

3. Sample magnetization

The temperature dependence of the magnetization in both the $ErFe_2$ and the $DyFe_2$ samples was measured at Warwick University with a magnetic balance using fields of up to 1.0 T and in each case the saturation magnetization was determined. The magnetization plots are shown in figure 2. The decomposition of the magnetic Compton profiles into the relative spin contributions from 3d, 4f and diffuse electron distributions at each temperature does not require the establishment of any absolute scale for the magnetization in the sample, only the assumption that the degree of saturation is the same throughout the temperature range. From figure 2 it can be seen that at room temperature and with an applied field of 0.5 T both samples are magnetized to 85–95% of their saturation value. This is only slightly decreased at lower temperatures.

4. Data analysis

The analysis of magnetic Compton scattering data is described fully in [16]. The data from each detector were processed separately and only combined at the final stage when it was clear that they contained no anomalies. The sum and difference spectra were corrected for the energy dependence of the scattering cross-section for charge and magnetic scattering

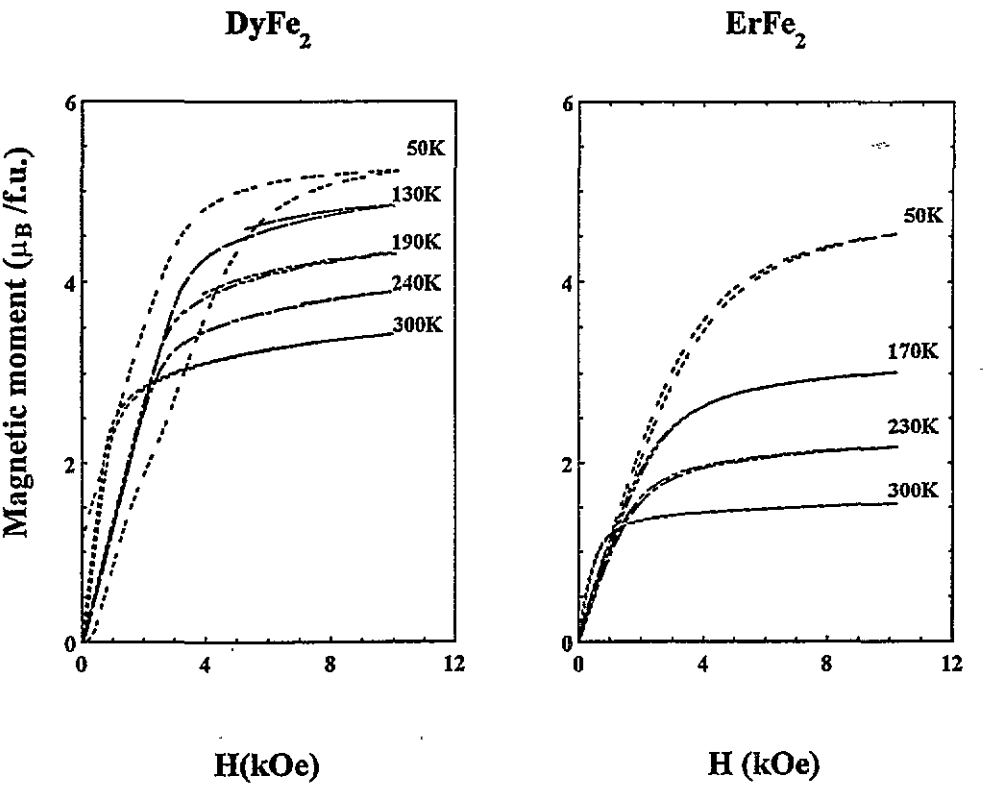

Figure 2. Magnetization curves of $ErFe_2$ and $DyFe_2$ as a function of temperature measured in units of Bohr magnetons (μ_B) per formula unit (FU) against an external magnetic field strength measured in kOe. A full hysteresis curve is shown for the 50 K measurement and partial hysteresis curves are shown at other temperatures.

using formulae derived in [17] and [18]. The spectra were also corrected for the energy dependence of absorption in the sample. Corrections for multiple scattering in magnetic Compton experiments have been shown to be small and can be neglected [19]. Subtraction of two normalized data sets, consisting of both charge and magnetic components, isolates the magnetic Compton profile because the charge profiles cancel out (see equations (5) to (7)). The difference profiles at high energies show no significant background contribution. The scale of the magnetic effect as represented by the ratio R is plotted as a function of temperature in figure 3. For $DyFe_2$ the magnetic effect remained negative at all temperatures measured. Extrapolation gave a compensation temperature, the temperature at which the magnetic effect would be zero, of almost 600 K. For $ErFe_2$ the magnetic effect was observed to be negative at low temperatures, reversing sign above a compensation temperature which in this case is approximately 50 K. The $HoFe_2$ results from earlier work [1] have been included in figure 3 and illustrate the superior quality of the present data which appear free from systematic errors. The errors in the present data can be wholly accounted for by Poisson statistics; this is primarily due to the magnetic field switching times being much faster than in the previous experiments. The data were analysed in terms of the Compton profiles derived from Hartree–Fock wavefunctions [20]. Such wavefunctions are a good approximation for the 4f rare-earth electrons, which are deeply embedded within the

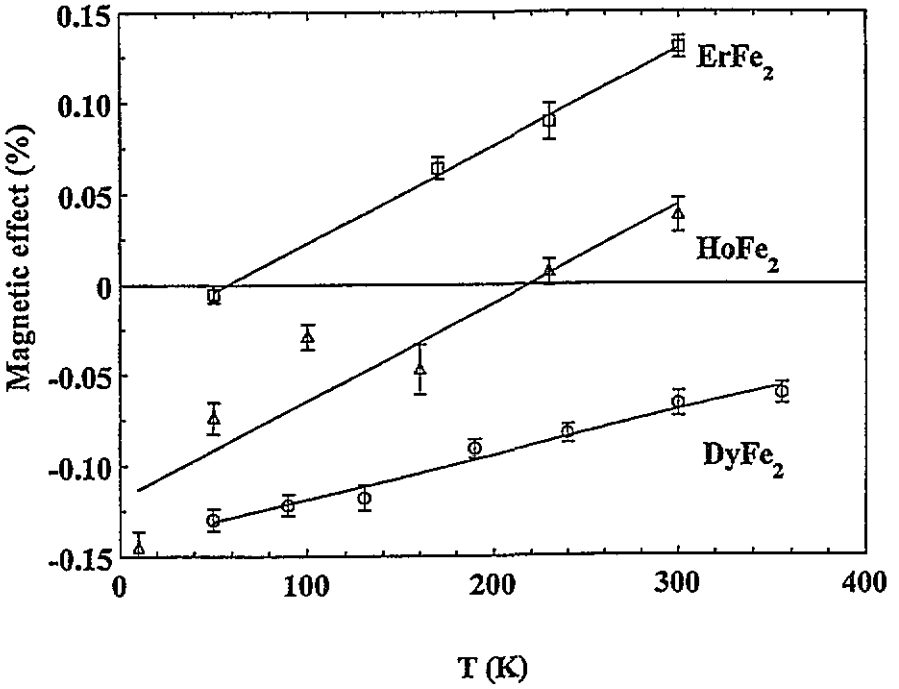

Figure 3. The temperature dependence of the total spin magnetic moment for $DyFe_2$, $ErFe_2$ and $HoFe_2$ measured as the percentage magnetic effect, R, as defined in the text.

atom. They are also a reasonable first approximation for the 3d electrons of Fe. A band-calculated momentum density would be preferable and should lead to some differences at low momentum ($|p_z| < 1$ au), such as those observed in pure Fe [21], although the difference would probably be negligible at the resolution of this experiment which is only 1.0 au FWHM. It is widely believed that the 'delocalized' spin moment in these compounds is centred upon the rare-earth ion. We had no free-atom Compton profile model available for such an orbital from the literature. However, in a previous study [16] a 5d Lu free-atom Compton profile had been used to model such an orbital in Ho. There it had been shown that, at the resolution of these experiments, there is no discernible difference between this model and the parabolic Compton profile of similar width, although the latter actually corresponds to a truly delocalized, free-electron-like density distribution. Both of these models were used and gave fits of similar quality and similar values for the diffuse moment. The analysis of the magnetic line shape into these component profiles works because the profiles are characteristically different functions of momentum. The 4f momentum distribution is much broader than the 3d, which in turn is much broader than the diffuse contribution. Examples of the magnetic Compton profiles for both $DyFe_2$ and $ErFe_2$ at both ends of the temperature ranges measured are shown in figure 4. The coupling between the moments on the rare-earth and Fe sites is antiferromagnetic and the diffuse component is aligned parallel to the rare-earth moment, which is negative in our convention. The individual theoretical profiles were fitted to the experimental data on the basis of yielding partial profiles whose sum was the best fit to the data. The area under each fitted partial profile is numerically equal to the spin moment per formula unit in Bohr magnetons as given by the normalization condition expressed by equation (4). Excellent fits were obtained for the 4f, Fe and diffuse

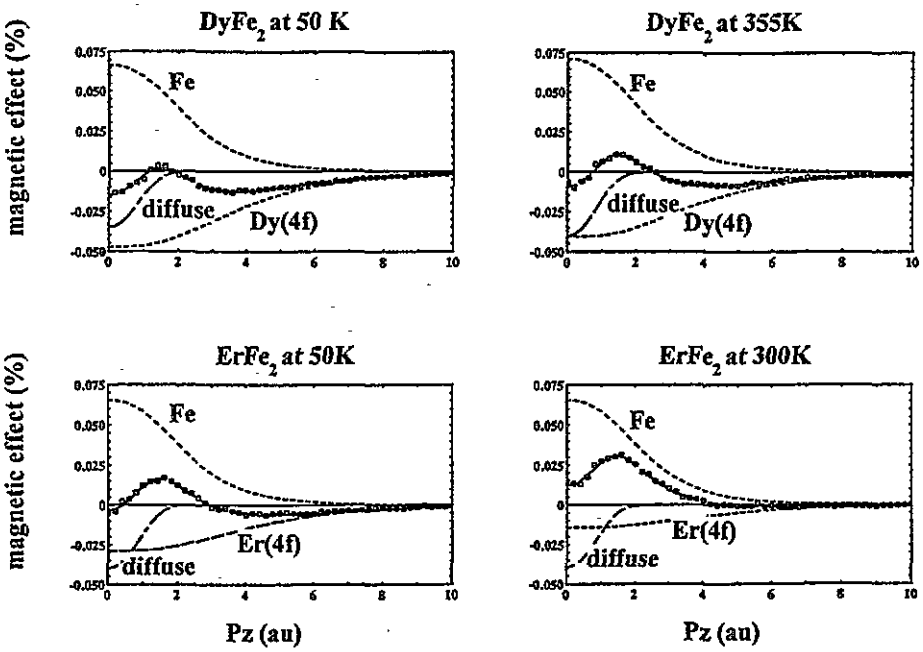

Figure 4. Magnetic Compton profiles of $DyFe_2$ and $ErFe_2$ at the extreme ends of the temperature range measured, plotted as magnetic effect (%) against electron momentum p_z in atomic units. The experimental data are the filled circles and the dashed lines are the iron, rare-earth and diffuse contributions. The theoretical profiles have been convoluted with a Gaussian of FWHM = 1.0 au to mimic the experimental resolution.

contribution at all temperatures as is evident from figures 4 and 5. Because the individual profiles used as basic functions to analyse the data differ so markedly, the partial areas under each component, and thus their magnetic moments, are well determined.

5. Temperature variation of the individual spin moments

Values for the individual Dy, Er, Fe and diffuse moments as a function of temperature were determined from the areas under each constituent profile and are shown in figure 5. It is necessary to know both the magnetization in the sample and the degree of circular polarization of the beam if absolute values for the spin moments are to be established. Although the latter can be predicted by modelling the behaviour of the elliptical multipole wiggler it is difficult to measure except by a magnetic Compton scattering experiment. The scale is therefore established by two procedures: (A) from a value for the Fe spin moment in $HoFe_2$ which is taken to be 1.85 μ_B per atom [15] used as an average value over the temperature range measured and (B) from independent measurements of the magnetic Compton profile of pure iron where the accepted spin moment value of 2.1 μ_B per atom was used to evaluate all the unknown geometric factors, together with the normalization condition for the charge scattering expressed by equation (2). An analysis of the above methods of establishing the scale is shown in figure 6. Procedure A is shown for both possibilities of modelling the diffuse component, that is by a free-electron profile or an empty orbital on the rare-earth site modelled by a 5d Lu orbit as explained earlier. As anticipated earlier there is

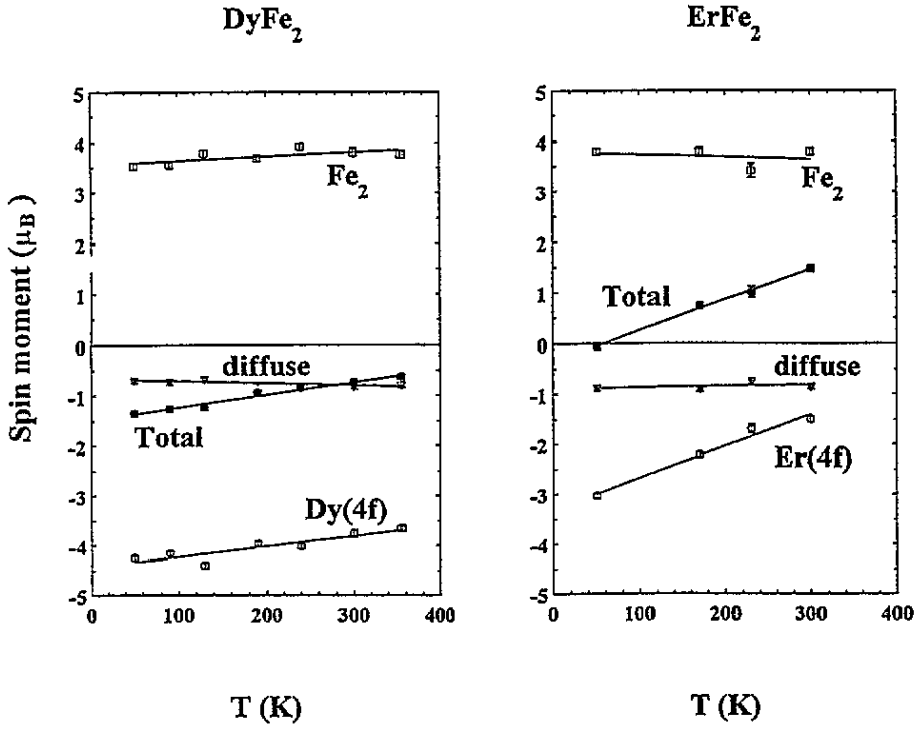

Figure 5. The magnetic spin moments of $DyFe_2$ and $ErFe_2$. The total spin moment has been separated into its rare-earth (4f), diffuse and iron (3d) moments. The graph has been plotted in units of Bohr magnetons against temperature in kelvin.

no significant difference between these two approaches. Likewise procedure B, which uses the Fe sample measurement, yields no discernible difference. This means that the analysis of the results is not sensitive to the precise method of establishing the absolute scale. An Fe moment of 1.85 μ_B together with the free-electron modelling of the diffuse component was, in fact, used. It is quite clear in both $ErFe_2$ and $DyFe_2$ that the temperature variation of the total spin moment is mirrored by the behaviour of the rare-earth 4f spin moment. From figure 5 it follows that the Dy spin moment falls from -4.25 ± 0.04 μ_B at 50 K to -3.66 ± 0.06 μ_B at 355 K. The diffuse moment is almost constant over this temperature range and between -0.6 and -0.7 μ_B. Both 4f and diffuse moments are opposite in sign to the Fe moment. The total spin moment of the $DyFe_2$ changes from -1.35 ± 0.06 μ_B at 50 K to -0.63 ± 0.06 μ_B at 355 K. A similar trend can be seen for $ErFe_2$, where there is a spin compensation temperature near 50 K, below which the total spin moment is negative. The uniform spin magnetic moment of iron over the temperature range examined may be explained in terms of sublattice interactions. In calculations on $HoFe_2$ [22] it has been shown that the Fe–Fe sublattice interactions are over three times stronger than the Ho–Fe interaction and forty times stronger than the Ho–Ho sublattice interactions, thus suggesting that the iron lattice may be less sensitive to temperature variations than the rare earth. Data taken from these experiments together with previous theoretical and experimental data are summarized in table 1.

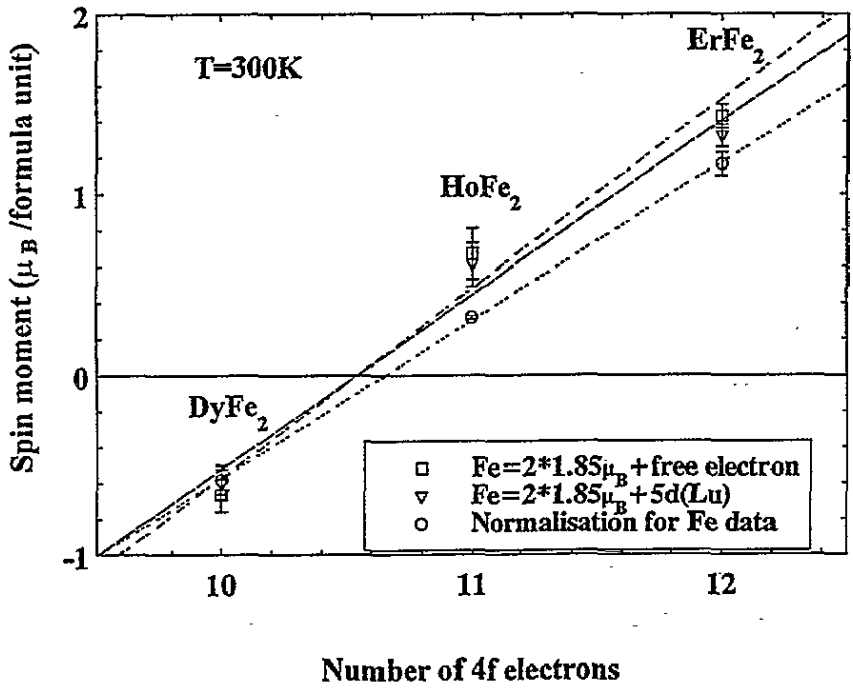

Figure 6. *Values of the total spin moments used as comparison of the normalization and diffuse* moment modelling methods for $DyFe_2$, $ErFe_2$ and $HoFe_2$ at a temperature of 300 K. Both possibilities for modelling the diffuse component, that is as a free-electron profile or 5d Lu orbit, together with using an Fe moment of 1.85 μ_B are shown together with the method using Fe sample measurements as explained earlier. There is no significant difference between these approaches. The graph has been plotted in units of Bohr magnetons against the number of 4f electrons.

6. Orbital magnetic moments

It is possible to deduce the orbital magnetic moments by subtracting the spin contribution from the bulk magnetization data. Such data were obtained for both samples using a vibrating-sample magnetometer at Warwick University and are shown in figure 2. From these data the total magnetization at temperatures between 50 and 300 K have been calculated and plotted in figure 7. Since the experiments were performed in a magnetic field of 0.5 T the bulk magnetization value corresponding to this applied field was used. Since only one measurement at each temperature was obtained the errors have been estimated from the hysteresis curves. The estimated saturation values are also shown. The relative signs of the spins have been calculated using Hund's rules. Since both $ErFe_2$ and $DyFe_2$ are ferrimagnetic the rare-earth and iron spins are opposite while the orbital and spin moments are in the same direction (since the shell is more than half full $J = L+S$). The 3d Fe orbital moment is quenched because it forms the outermost shell and is therefore fully locked into the surrounding crystalline field and is unable to orientate itself with the external magnetic field. The electron spin can freely orientate itself with the external magnetic field because it has no direct interaction with the crystalline field. On the other hand, the paramagnetic 4f rare-earth electrons are in an inner shell and are shielded from the crystalline field by the 5s and 5p shells. This leaves the rare-earth orbital moment free to orientate itself

Table 1. A summary of the experimentally determined values for magnetic moments in $DyFe_2$ and $ErFe_2$. The values given are for the spin moment on both Fe sites, the diffuse spin moment, the rare-earth spin moment and the total spin moment together with the calculated orbital moment and the bulk sample measurements at both 0.5 T and at saturation. The values for 0 K have been extrapolated from finite-temperature measurements by using a least-squares regression for comparison with previous theoretical and experimental data.

Partial moment	$DyFe_2$ 0K	Previous Results (0K)	$DyFe_2$ 300K
2*Fe Spin	+3.55 ±0.06	+3.60 ±0.08 [23]	+3.79 ±0.11
Diffuse Spin	-0.67 ±0.05		-0.82 ±0.05
RE Spin	-4.44 ±0.04		-3.76 ±0.08
Total Spin	-1.48 ±0.06		-0.74 ±0.08
Orbital	-3.89 ±0.26		-2.37 ±0.28
Bulk 0.5T	-5.4 ±0.2		-3.1 ±0.2
Bulk Sat	-6.0 ±0.2	~-6.7 [24]; -4.91 [23]	-3.6 ±0.2
		-6.9 [15]; -5.75 [25]	

Partial moment	$ErFe_2$ 0K	Previous Results (0K)	$ErFe_2$ 300K
2*Fe Spin	+3.78 ±0.07	+3.60 ±0.08 [23]	+3.80 ±0.08
Diffuse Spin	-0.89 ±0.06		-0.85 ±0.06
RE Spin	-3.31 ±0.05		-1.50 ±0.06
Total Spin	-0.35 ±0.06		+1.48 ±0.07
Orbital	-4.01 ±0.26		-3.80 ±0.26
Bulk 0.5T	-4.4 ±0.2		-1.5 ±0.2
Bulk Sat	-5.3 ±0.2	~-5.9 [24]; -4.75 [23]	-1.7 ±0.2
		-5.8 [15]; -4.85 [25]	

with an external field in a similar way to that in which a free iron moment would. From the experimental results the diffuse moment is shown to be smaller than the rare-earth moment. The above argument for calculating the relative directions of the moments can be summarized as

$$\text{Bulk moment} = [\text{Dy} + \text{Diff}]^{\downarrow}_{\text{orb}} + [\text{Dy}^{\downarrow} + \text{Diff}^{\downarrow} + \text{Fe}^{\uparrow}]_{\text{spin}} \tag{8}$$

where the convention has been to take the iron spin moment as being positive. This analysis enables the calculation of the orbital moments for both $DyFe_2$ and $ErFe_2$ shown in figure 7 to be performed. The orbital moments are determined by this method to better than ±10%. Extrapolation using a least-squares regression gives the estimated bulk magnetic saturation values at 0 K for $DyFe_2$ and $ErFe_2$ as $6.0 \pm 0.2\ \mu_B$ and $5.3 \pm 0.2\ \mu_B$ respectively. These values can be compared with the theoretical values [25] of approximately $5.75\ \mu_B$ for $DyFe_2$ and $4.85\ \mu_B$ for $ErFe_2$. The errors in the orbital moments directly relate to the errors in the VSM measurements which may be a conservative overestimation.

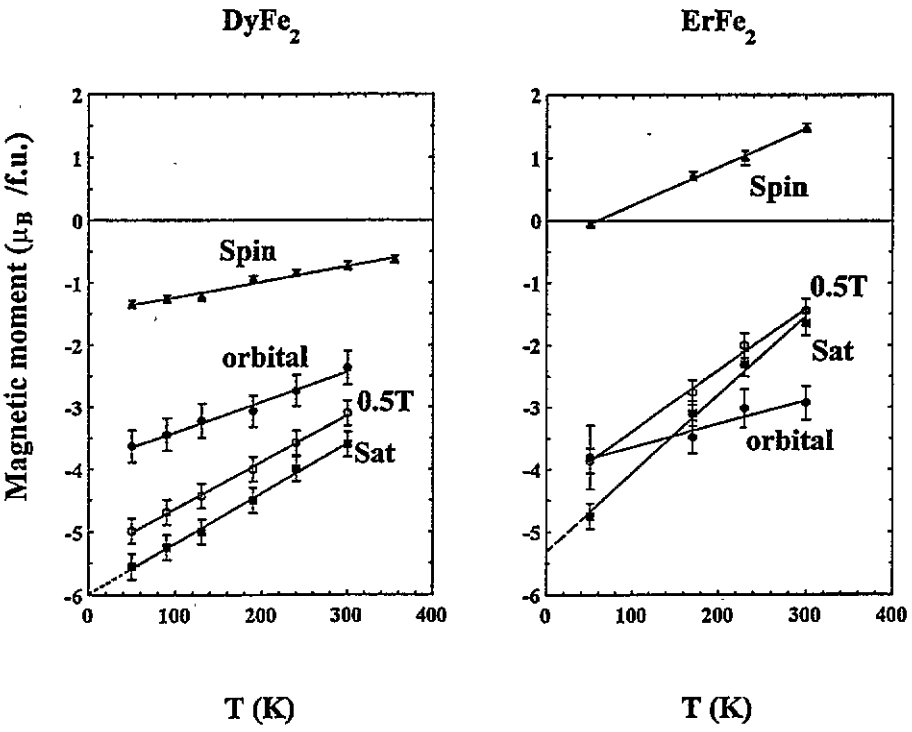

Figure 7. The calculation of the orbital moment as a function of temperature of $DyFe_2$ and $ErFe_2$. The total bulk moment was measured at 0.5 T on a vibrating-sample magnetometer; this field value is the value used for the spin measurements. The orbital moments are calculated as the total bulk moments minus the spin moments, taking into account the relative directions calculated by Hund's rules. The figure shows plots of bulk measurements at 0.5 T and at saturation, Sat, as well as the spin and orbital moments. The magnetic moment in units of μ_B/formula unit is plotted against temperature in units of kelvin.

7. Summary

The magnetic Compton profiles of $DyFe_2$ and $ErFe_2$ have been analysed in terms of the contributions from 4f, 3d and diffuse electrons. The temperature dependence of the spin moment is primarily associated with the change of the rare-earth 4f moment. The measurements confirm a value of approximately 0.7 to 1.0 μ_B for the diffuse moment throughout this temperature range, in agreement with previous experiments on $HoFe_2$ [1]. This study shows the crucial importance of good signal averaging in magnetic Compton scattering experiments. There is a conflict between the need to saturate samples magnetically and the need to reverse the magnetic field frequently. It is unlikely that low-temperature experiments on hard ferromagnets can be entirely successful with either electromagnets (low magnetization) or superconducting magnets (poor signal averaging). Therefore techniques which reverse the hand of polarization deserve attention. This might be accomplished by either modulating the field in an insertion device or moving the sample from above to below the orbital plane. If these methods are developed it is clear that both orbital and spin moments can be determined in a range of interesting actinide and rare-earth materials.

Individual spin moments for both $DyFe_2$ and $ErFe_2$ have been calculated with very good statistics and information about orbital moments has been deduced via comparison

with bulk magnetization data. If obtaining the magnetic Compton profiles of hard magnetic materials becomes achievable it appears from this work that both spin and orbital moments can be deduced from this type of measurement.

Acknowledgments

The samples were made in the Department of Metallurgy and Materials at the University of Birmingham, UK. This work is supported by grants from the EPSRC (formally the SERC) and the British Council in Japan and forms part of a programme of x-ray studies of magnetic materials supported by the European Community Human Capital and Mobility initiative. We are grateful to the Director of the Photon Factory at KEK for allocating beamtime to this project under proposal number 90-231. The VSM measurements were carried out at Warwick University by Dr C V Tomy.

References

[1] Żukowski E, Cooper M J, Timms D N, Armstrong R, Itoh F, Sakurai H, Tanaka Y, Ito M, Kawata H and Bateson R 1994 *J. Phys. Soc. Japan.* at press
[2] Sakai N and Ono K 1976 *Phys. Rev. Lett.* **37** 351
[3] Holt R S and Cooper M J 1983 *Nucl. Instrum. Methods* **213** 447
[4] Sakai N, Terashima O and Sekizawa H 1984 *Nucl. Instrum. Methods* **221** 419
[5] Holt R S, Laundy D, Cardwell D A, Cooper M J, Naylor T, Manninen S and Hatton P 1986 *Nucl. Instrum. Methods* A **243** 608
[6] Cooper M J, Laundy D, Cardwell D A, Timms D N, Holt R S and Clark G 1986 *Phys. Rev.* B **34** 5984
[7] Platzman P M and Tzoar N 1970 *Phys. Rev.* B **2** 3556
[8] Timms D N, Cooper M J, Holt R S, Itoh F, Kobayasi T and Nara H 1990 *J. Phys.: Condens. Matter* **2** 10517
[9] Cooper M J 1985 *Rep. Prog. Phys.* **48** 415
[10] Cooper M J, Żukowski E, Collins S P, Timms D N, Itoh F and Sakurai H 1992 *J. Phys.: Condens. Matter* **4** L399
[11] Timms D N, Żukowski E, Cooper M J, Laundy D, Collins S P, Itoh F, Sakurai H, Iwazumi T, Kawata H, Ito M, Sakai N and Tanaka Y 1993 *J. Phys. Soc. Japan* **62** 1716
[12] Yamamoto S, Kawata H, Kitamura H and Ando M 1989 *Phys. Rev. Lett.* **62** 2672
[13] Kawata H, Miyahara T, Yamamoto S, Shioya T, Kitamura H, Sato S, Asaoka S, Kanaya N, Iida A, Mikuni A, Sato M, Iwazumi T, Kitajima Y and Ando M 1989 *Rev. Sci. Instrum.* **60** 1885
[14] Kawata H, Sato M, Iwazumi T, Ando M, Sakai N, Ito M, Tanaka Y, Shiotani N, Itoh F, Sakurai H, Sakurai Y, Watanabe Y and Nanao S 1991 *Rev. Sci. Instrum.* **62** 2109
[15] Brooks M S S, Nordström L and Johansson B 1991 *J. Phys.: Condens. Matter* **3** 2357
[16] Żukowski E, Collins S P, Cooper M J, Timms D N, Itoh F, Sakurai H, Kawata H, Tanaka Y and Malinowski A 1993 *J. Phys.: Condens. Matter* **5** 4077
[17] Ribberfors R 1975 *Phys. Rev.* B **12** 2067, 3136
[18] Lipps F W and Tolhoek H A 1954 *Physica* **20** 85, 395
[19] Sakai N 1987 *J. Phys. Soc. Japan* **56** 2477
[20] Biggs F, Mendelsohn L B and Mann J B 1975 *At. Data Nucl. Data Tables* **16** 201
[21] Kubo Y and Asano S 1990 *Phys. Rev.* B **42** 4431
[22] Burzo E 1971 *Z. Phys.* **32** 127
[23] Taylor and Darby (ed) 1972 *Physics of Rare Earth Solids* (New York: Chapman and Hall)
[24] Clark A E 1980 *Ferromagnetic Materials* ed E P Wohlfarth (Amsterdam: North-Holland) p 297
[25] Buschow K H J 1977 *Rep. Prog. Phys.* **40** 1179